Article

Nickel Nanoparticles Decorated on Glucose-Derived Carbon Spheres as a Novel, Non-Palladium Catalyst for Epoxidation of Olefin

Mosaed S. Alhumaimess

Chemistry Department, College of Science, Jouf University, Sakaka P.O. Box 2014, Saudi Arabia; mosaed@ju.edu.sa

Abstract: Carbon spheres supporting nickel nanoparticles (NPs), generated by the integration of hydrothermal and microwave irradiation techniques, catalyzed the epoxidation of 1-octene, cyclooctene, styrene, allyl alcohol, and cyclohexene. The average particle sizes of the carbon spheres (CSs) and nickel oxide species immobilized on the CSs were 240 nm and 26 nm, respectively. The fabricated composites incorporating nickel NPs showed higher activity in the cyclohexene epoxidation process. The cyclohexene conversion was enhanced by raising the Ni loading to 10%. Within 14 h, the cyclohexene conversion had grown to 98%. This robust catalytic activity can be attributed to the efficient distribution of Ni species on the CSs, the facile lowering of the surface, and the development of uniformly nanosized species. The composite exhibited good recyclability across at least five cycles (which is not a simple task involving nickel-nanoparticle-based catalysts that are employed in water), and no nickel species leached into the solution, making the total system environmentally benign and cost-effective.

Keywords: epoxidation; carbon; NiO; hydrothermal; glucose

1. Introduction

The catalytic performance of metallic NPs is highly influenced by their dispersion and size on the support. Small NPs with a homogeneous dispersion have the maximum active surface area. The metal–support interaction has an additional impact on the catalyst's electronic structure and stability. As a result, a successful catalyst must meet a set of standards and possess certain characteristics. Electronic properties, high durability, the existence of modified moieties to combine with catalyst NPs, a porous texture to allow reagent entry, a simple synthesis procedure, and low cost are just a few of them [1–3].

Carbon-based nanomaterials, such as carbon nanotubes, activated carbon, carbon spheres, and graphene, are among the catalytic supports that have been extensively studied [4–10]. Carbon black is the most widely studied although it has significant drawbacks, such as corrosion in the reaction media and the degradation of the catalytic performance due to NPs detaching. A wide range of carbon-based nanomaterials have been evaluated in order to find a catalyst support that meets the aforementioned requirements. Carbon spheres are one type of carbon-based materials that has uniform geometries and large surface areas; that is of great significance. Furthermore, diverse fabrication parameters can be applied to control the textural properties and the form of porosity through a reasonable growth process. Carbon spheres have been employed in a broad range of implementations [11]. Therefore, using carbon spheres as supports for catalytic application technologies is more promising due to lower costs and better durability.

Because of their enormous economic interest, epoxides are regarded as one of the most significant intermediates in applied chemistry [12,13]. Polymers, surfactants, paints, medicines, insecticides, cosmetics, textiles, and detergents all employ them [14]. As a

result, efforts have been made to find or manufacture catalysts capable of producing epoxides [15]. Because of their high catalytic efficiency, traditional epoxidation catalysts containing transition-metal complexes and soluble transition-metal salts have been widely utilized for the homogeneous epoxidation of organic molecules, such as styrene, cyclohexene, and cyclooctene [16,17]. However, the use of these catalysts is restricted by their massive costs, as well as by the difficulty in removing them from the reaction mixture. Furthermore, to produce epoxides from olefins, the best catalysts primarily focus on a variety of homogeneous and heterogeneous materials [18–22]. However, in practical commercial processes, the aforementioned catalysts suffer from issues, such as high costs, limited stability, and low selectivity. As a result, a variety of approaches and tactics for immobilizing homogeneous catalysts on insoluble substrates have been investigated. Non-noble-metal nanocatalysts have various benefits over single-component noble-metal nanocatalysts. First, the immobilization of non-noble-metals-based catalysts aids in cost reduction, as excessive costs have been a critical threat for all of the commercial technologies. Non-noble constituents operate as promoters or supports in hybrid catalysts, lowering the concentration of noble metals significantly. Reusable, heterogeneous catalysts based on transition metals are therefore far more appealing from a technical, economical, and environment standpoint, particularly for industrial processes [23,24]. Many attempts have been undertaken in recent years to develop new catalytic systems based on the utilization of low-cost and non-noble metals, with a particular focus on the creation of catalysts for olefin epoxidation. Nasseri et al. [16] used silica to immobilize Fe_3O_4 NPs, and the resulting catalyst was used to epoxidate numerous alkenes and cycloalkenes in moderate conditions. Ghiami et al. [17] employed $FeNi_3$ NPs grafted onto silica in alkene epoxidation. Bhaumik et al. also used silica to immobilize Co(III) [18] and Cr [19], and the fabricated catalysts were successfully applied in oxidation processes. Held et al. studied vanadium-integrated mesocellular silica foams to catalyze propene epoxidation [20]. As can be noted, developing an efficient, selective, and durable catalyst for the epoxidation process continues to pique researchers' interests.

In this research, various amounts of Ni content were immobilized on carbon spheres (Ni/CSPs). The nanocatalysts were fabricated by a simple, tunable, and cost-effective hydrothermal approach, and their catalytic performance in olefin epoxidation was investigated using various olefin substrates. In addition, this research looked at the kinetic results of olefin epoxidation using Ni/CSP NPs as a catalyst under various experimental conditions.

2. Results

2.1. Spectroscopic Assessment

FT-IR spectra of the prepared CSs and Ni@CS composites are illustrated in Figure 1a. The spectrum of the as-synthesized CSs calcined at 700 °C, displaying the following absorption bands: a wide absorption peak from 3000 to 3500 cm^{-1} due to O-H stretching, a weak peak at 2900 cm^{-1} assigned to aliphatic C-H stretching modes; characteristic bands at 1614 and 1717 cm^{-1} are attributed to C=C and C=O modes, respectively, and bands between 500 and 900 cm^{-1} are mainly related to C-H bending modes. The FT-IR spectra of the (5 and 10%) Ni@CS composites are virtually identical. However, the absorption bands' growth was reduced after the loading of the Ni NPs, implying that the CSs' surface functionality remained intact.

Figure 1b shows the wide-angle XRD patterns of the pure CSs and the Ni@CS composites containing different Ni content. The wide diffraction peaks at 2θ = 21.8°, 25.8°, and 26.3° for pure CSs, 5% Ni@CSs, and 10% Ni@CSs, respectively, were attributed to the graphitic matrix. In addition, the intensity of the diffraction peaks gradually increased with the increase in Ni content. The diffraction peaks at 37.2°, 43.3°, 63.2°, and 75.3° are attributed to the (111), (200), (220), and (311) planes, respectively, of NiO with a cubic structure (JCPDS 78-0423) [7].
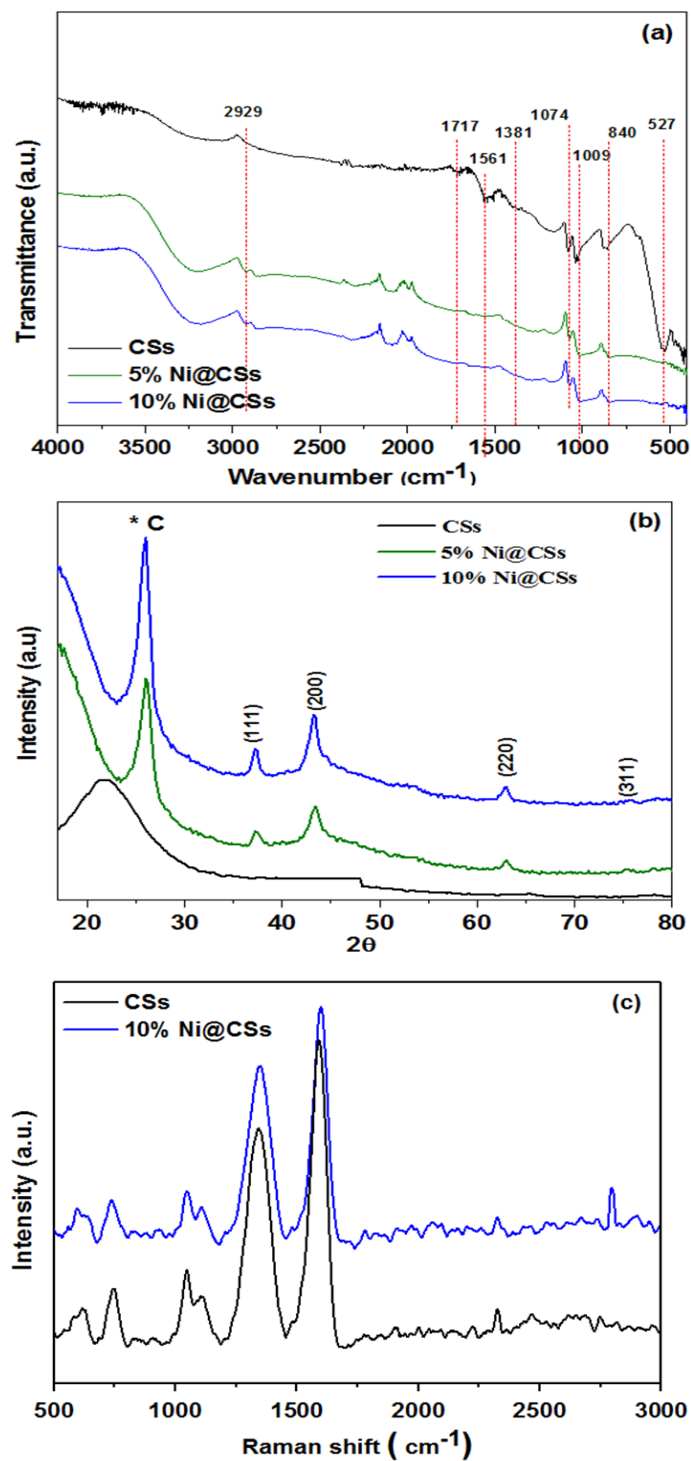
Figure 1. (**a**) FT−IR spectra, (**b**) XRD diffraction patterns, and (**c**) Raman spectra of CSs and Ni@CS composites.

Figure 1c shows two distinct bands in the Raman spectrum of the CSs, the D peak at 1343 cm^{-1} and the G peak at 1585 cm^{-1}, which were ascribed to sp^3 and sp^2-carbon, respectively, [23]. The Raman spectrum of the Ni@CS composite showed identical bands at 1348 and 1598 cm^{-1}, which were likewise attributed to the G and D modes. The intensity ratio (ID/IG) was used to measure the quality of the carbon matrix because this ratio is almost zero for highly ordered carbon [24]. The ID/IG value of the CSs loaded with Ni

NPs increased from 0.29 of the pure CSs to 0.81 of the Ni@CSs, implying an increase in defects in the carbon matrix, which could boost the catalytic performance.

The atomic absorption spectroscopy (AAS) was used to estimate the actual concentrations of Ni immobilized on the CSs (Table 1). The actual concentrations were observed as being lower than the calculated values, which could be assigned to the leaching of weakly bound Ni NPs during the preparation procedure.

Table 1. Binding energies and surface contributions of C1s, O1s, and Ni2p of the catalysts.

Sample	C1s [a]	O1s [a]	Ni2p [a]	Actual at% Ni	Found at% Ni [b]
CSs	283.3 (86.1)	530.8 (13.64)	-	-	-
5% Ni@CSs	284.1 (55.1)	531.2 (6.50)	856 (0.9)	5	4.93
10% Ni@CSs	284.2 (84.1)	531.9 (14.40)	856 (1.5)	10	9.20

[a] The values in parentheses represent the atomic % of the elements. [b] The atomic percentage of the Ni element, as determined by AAS.

The valence state and electron binding energy of Ni immobilized on the carbon spheres were determined using XPS. The O1s region, the C1s region, and the 2p region of Ni were examined using the Gaussian–Lorentzian approach, as displayed in Figure 2 and Table 1. The XPS spectrum of high-resolution C1s (Figure 2a) reveals three peaks at 284, 286.9, and 288.6 eV, which related to the C=C, C–O, and C=O moieties, respectively. The (C-O-C) and hydroxyl (OH) binding energies were 531.4 and 531.1 eV, respectively, in the O1s (Figure 2b). The high-resolution Ni2p spectrum in Figure 2c shows two edge-splits by spin coupling: the 2p3/2 major peak at approximately 855.3 eV and its shoulder at about 863 eV, and the fitting 2p1/2 peak at 872.5 eV and its shoulder at 878.5 eV, indicating the presence of NiO species [25]. The surface atomic composition obtained from the XPS data is also shown in Table 1. The concentration of Ni on the CSs' surface is found to be lower than that in the bulk when compared to the Ni bulk concentration determined by AAS.

2.2. Morphology Assessment

HRTEM revealed the morphology and particle size distribution histograms of the CS and Ni@CS samples, as shown in Figure 3. The CSs with flat surfaces were uniformly dispersed and had well-defined, homogeneous, spherical shapes, as depicted. Furthermore, after the immobilization of Ni NPs, the shape of the CSs was unaffected. HRTEM images were used also to determine the particle size distribution and average particle size. The average particle size of the CSs was 240 nm (Figure 3B), and the average particle size of nickel oxide species immobilized on the CSs was 26 nm (Figure 3D). Furthermore, the TEM image of the Ni@CSs displays the existence of evenly distributed NiO species on the carbon spheres with no agglomeration into big clusters.

2.3. Catalytic Performance

The CSs and 5% Ni@CSs and 10% Ni@CS composites were examined in the epoxidation of cyclohexene using an oxidant of $NaHCO_3/H_2O_2$ in the presence of acetonitrile (Scheme 1). The findings of the cyclohexene epoxidation reaction revealed that the major epoxidation products were 1,2-cyclohexanediol and 1,2-epoxycyclohexane, as well as tiny by-product quantities of 2-cyclohexenol and 2-cyclohexenone compounds. Figure 4a shows the cyclohexene conversion at different time intervals at 353 K using CSs and 5% Ni@CS and 10% Ni@CS composites under the reaction conditions catalyst (50 mg) using H_2O_2-$NaHCO_3$ (pH = 8). The results indicated that the CSs had poor activity, with a cyclohexene conversion of only 21% over the 16-h period. The fabricated composites incorporating nickel NPs, on the other hand, showed higher activity in the cyclohexene epoxidation process. By raising the Ni loading to 10%, the cyclohexene conversion was enhanced. Within 14 h, the cyclohexene conversion had grown and had reached a plateau. The selectivity for 1,2-epoxycyclohexane, on the other hand, did not really match the pattern of the cyclohexene conversion (Figure 4b). After 8 h of reaction, the selectivity dropped to 80%,

and then it dropped to 25% after 16 h. The fruitful oxidation of cyclohexene into 1,2 epoxy-cyclohexane (98%) along with the 1,2-cyclohexanediol molecule (0.73%) was responsible for the inverse relationship with time to, 1,2 epoxycyclohexane (98%), 1,2 cyclohexanediol (0.73%), 2-cyclohexenol (0.87%), and 2-cyclohexenone (0.4%).
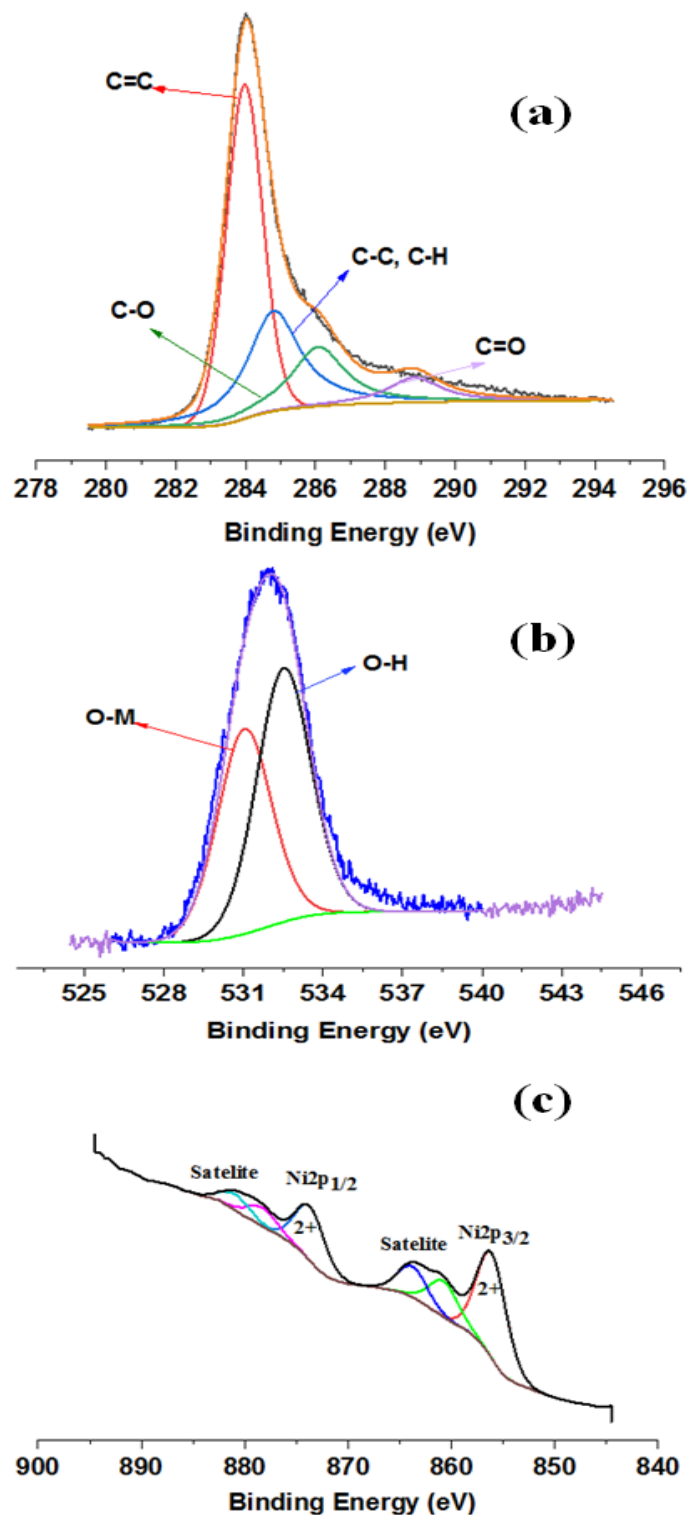

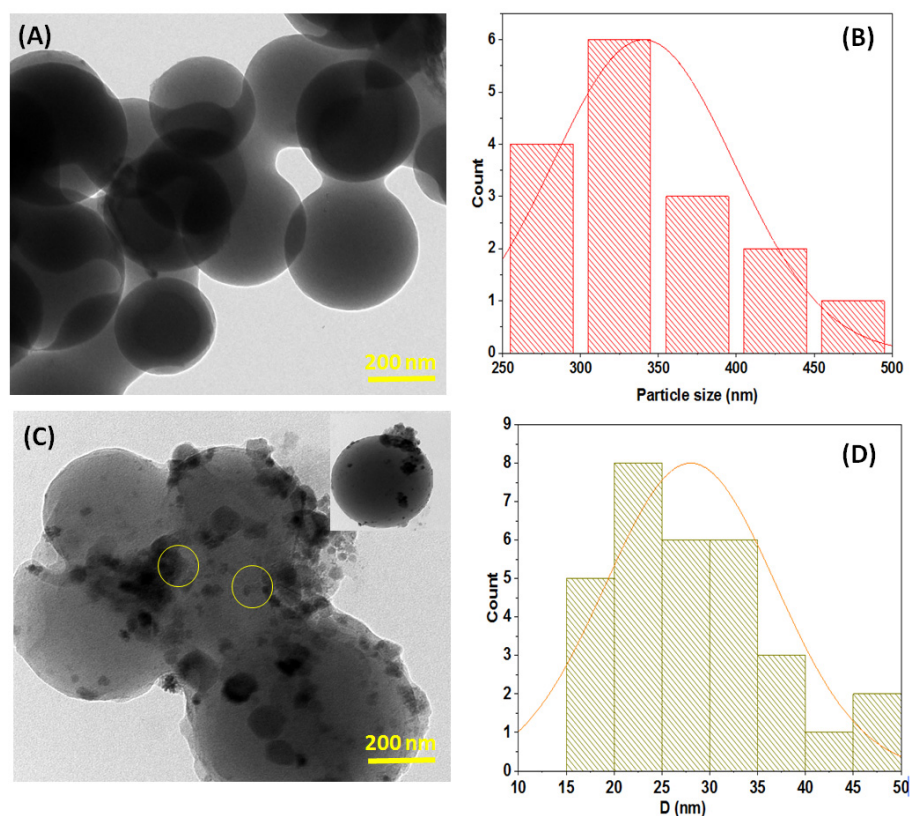**Figure 2.** XPS spectra of Ni@CSs composite: C1s (**a**), O1s (**b**), and Ni 2p (**c**).

Figure 3. HRTEM and particle size distribution histogram of CSs (**A**,**B**) and Ni@CS composites (**C**,**D**).

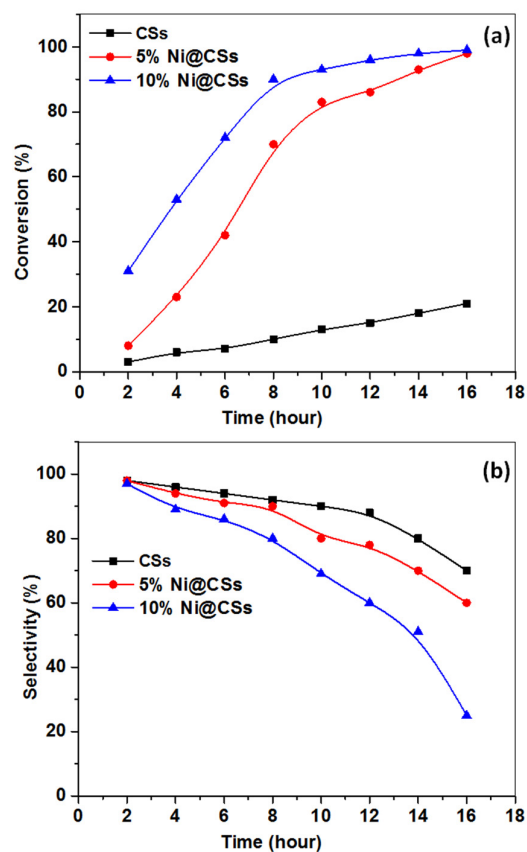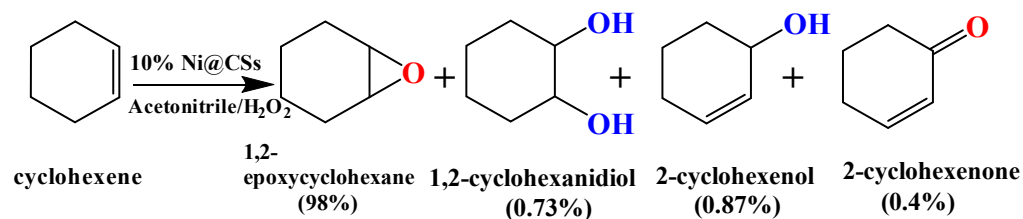**Figure 4.** (**a**) Conversion (%) of cyclohexene, and (**b**) selectivity (%) of cyclohexene oxide using 10% Ni@CSs composite (50 mg catalyst, 353 K, pH = 8, and 14 h).

Scheme 1. Reaction scheme of the catalytic epoxidation of cyclohexene 10% Ni@CSs.

2.3.1. Impact of Catalyst Dose

Figure 5a displays the influence of composite dose on the epoxidation of cyclohexene after 14 h at 353 K with a pH equal to 8. The 10% Ni@CS catalyst dose was initiated with 10 mg and then extended to 20 mg. The comparable conversions were discovered to be 20% and 43%, respectively. The cyclohexene conversion increased to 98% when the catalyst dose was extended to 50 mg. When the quantity of the catalyst is increased, the number of active catalyst sites needed to complete the reaction increases. When the catalyst dose was raised from 50 to 70 mg, the cyclohexene conversion percentage remarkably declined from 98 to 83%, owing to the greater number of active sites in the catalyst generating more by-products.
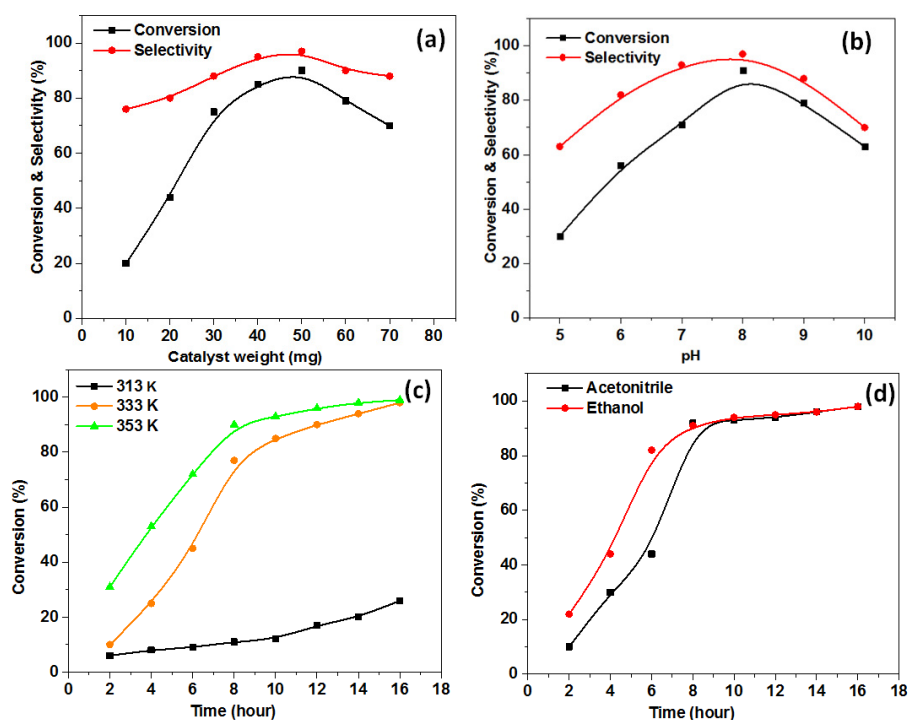

Figure 5. Optimum reaction conditions of the catalytic epoxidation of cyclohexene using 10% Ni@CSs composite: (**a**) effect of catalyst dose (353 K, pH = 8, and 14 h); (**b**) effect of pH (50 mg catalyst, 353 K, and 14 h); (**c**) effect of temperature (50 mg catalyst, pH = 8, and 14 h); and (**d**) effect of solvent (50 mg catalyst, 353 K, pH = 8).

2.3.2. Impact of pH

Initially, an effervescence is observed in the absence of the catalyst when a mixture of H_2O_2 and $NaHCO_3$ is added to the cyclohexene and acetonitrile mixture, and by analyzing the arising gas, we identified it as oxygen, which describes the epoxidation process' decline. In Figure 5b, the ratio of H_2O_2 to mol of $NaHCO_3$ was varied to achieve pH values ranging from 5 to 10. After 14 h at pH 8, the impact of the pH value on the epoxidation performance at 353 K was determined. In the epoxidation process catalyzed by 10% Ni@CSs

to activate hydrogen peroxide, the introduction of $NaHCO_3$ was completely significant, with roughly 1.3% cyclohexene conversion produced after 2 h in the absence of $NaHCO_3$. The cyclohexene conversion increased from 30% to 72% when the reaction pH was raised from 5 to 7. Furthermore, at pH 8, there was a significant rise in cyclohexene conversion of up to 90%. At a pH of 8, the volcano-curve with pH can be associated with the production of adequate amounts of HCO_4^- species. Because peroxymonocarbonate (HCO_4) is the most powerful in boosting the process, the H_2O_2 and $NaHCO_3$ mixture displays a high level of efficiency towards the synthesis of epoxide according to Yao and Richardson [25]. Once the $NaHCO_3$ concentration rose to a pH of 10, however, epoxidation dropped to about 58%.

2.3.3. Impact of the Epoxidation Temperature

Figure 5c shows the cyclohexene conversion to epoxide at the various temperatures of 313, 333, and 353 K. When compared to other temperatures, 353 K produced the highest cyclohexene conversion. Because heat accelerates reactant removal from the catalyst's surface, reaction kinetics improve as temperature increases, resulting in more collisions and a higher rate of reaction.

2.3.4. Impact of the Solvents

The choice of a proper solvent for the epoxidation is one of the most important factors influencing the epoxidation of cyclohexene to the corresponding epoxide. Figure 5d shows the effect of several solvents on the conversion, along with the selectivity of cyclohexene to cyclohexene epoxide. As can be seen, when utilizing ethanol, the cyclohexene conversion against time was faster than when using acetonitrile (reaching 83% compared to 41% in 6 h). If ethyl alcohol is used, selectivity drops dramatically over time, possibly because the alcohol stimulates the ring opening of the epoxide [26]. Furthermore, acetonitrile, a somewhat basic solvent, has been shown to prevent the conversion of styrene oxide to benzaldehyde [27]. As a result, utilizing acetonitrile as a solvent yields the greatest results.
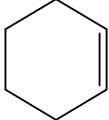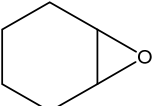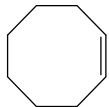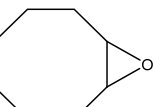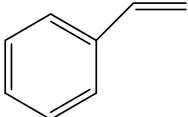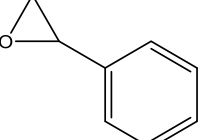
2.3.5. The Scope for Epoxidation Reaction

The conversion and selectivity of a wider spectrum of alkenes at 353 K, pH 8, with the use of acetonitrile are presented in Table 2. The 10% Ni@CSs appeared to be the most powerful of the tested catalysts; hence, that was chosen as the catalyst for the subsequent epoxidation measurements. It is obvious from the table that the cyclooctene and cyclohexene exhibited the highest conversions. The low-basicity of the π-electron moiety, steric hindrance, or the tautomerization phenomenon may be to blame for the epoxidation's decreased electrophilic cycloaddition [28–30]. The cyclohexene conversion was 98% (for cyclohexene), 99% (for cyclooctene), 89% (for styrene), 93% (for oct-1-ene), and 60% (for prop-2-en-1-ol).
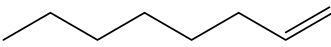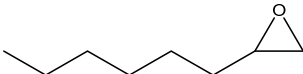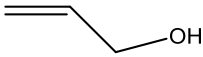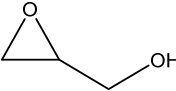
2.3.6. Recycling Process

Catalyst durability is a major issue in heterogeneous catalysis as it provides for more cost-effective and ecologically friendly processes. As a result, we investigated the reusability of the catalyst in the epoxidation of cyclohexene (Figure 6). The catalyst can be readily separated by filtration, rinsed with ethanol, dried, and reutilized for subsequent reactions after each reaction cycle. Obviously, the catalyst can be reused at least five times without losing its catalytic performance. Furthermore, applying the AAS assessment, nickel species detached from the carbon spheres' surfaces was investigated in the reaction mixture after the process was completed. The results revealed no trace amounts of nickel leached into the solution. The groups' functionality on the surface of carbon spheres provides potential interacting sites with nickel species, thus offering facile catalyst reusability and minimizing metal detachment.

Table 2. Substrates scope of olefins for the epoxidation reaction catalyzed by 10% Ni@CSs (50 mg catalyst, 353 K, pH = 8, and 14 h).

Olefin	Time (h)	Product	Conversion (%)	Selectivity (%)
Cyclohexene	14	Cyclohexene epoxide	98	55
Cyclooctene	14	Cyclooctene epoxide	99	93
styrene	14	Styrene epoxide	89	80
oct-1-ene	14	Octe-1-ene epoxide	93	80
Prop-2-en-1-ol	14	Prop-2-en-1-ol epoxide	60	91
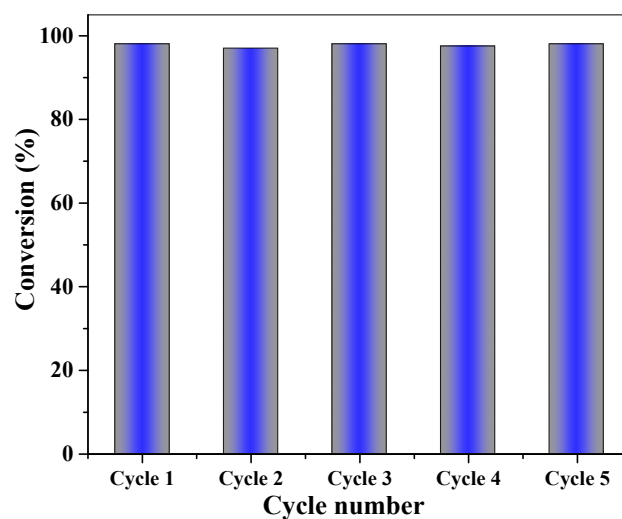
Figure 6. Recycling experiment using 10% Ni@CSs composite catalyst in cyclohexene epoxidation (50 mg catalyst, 353 K, pH = 8, and 14 h).

2.3.7. Comparison Assessment

The problem with obtaining an acceptable comparison stems from the fact that only a small number of studies have addressed the heterogeneous epoxidation of cyclohexene utilizing carbon spheres. We compared our results to those cited in the literature for a nickel-based carbon sphere catalyst [31–36]. Table 3 shows the findings regarding cyclohexene oxidation. It can be seen that the results acquired in this investigation were more active than those of previous publication.

Table 3. Catalytic activity of various heterogeneous catalysts in cyclohexene epoxidation.

Catalyst	Time (h)	Conversion/%	Reference
V (IV) Schiff bases/GO	10	92	[31]
Cu (II) Schiff bases/Monolith	24	82	[32]
RuO2/Meso-TiO2	3	35	[33]
Bulk NiO	8	13	[34]
NiO/MCM-41	3	62	[35]
Pd Schiff base/MCM-41	16	74.5	[36]
Ni@CSs	0.5	98	This Work

3. Materials and Methods

3.1. Chemicals

The glucose (D(+), ≥ 99.5) used to prepare the CSs, potassium carbonate (K_2CO_3, $\geq 99.9\%$), nickel(III) nitrate hexahydrate ($Ni(NO_3)_2$, $6H_2O$, $\geq 99.9\%$), H_2O_2 (30% in H_2O), polyvinyl alcohol (PVA) (Mw = 10,000, 80%), cyclohexene ($\geq 99.0\%$), $NaHCO_3$ ($\geq 99\%$), cyclohexene (96%), 1-hexene (91%), cyclooctene (≥ 99), and styrene (≥ 99) were procured from Sigma-Aldrich Co.(St. Louis, MO, USA). Hydrazine hydrate (80% solution in water) was obtained from Merck, Germany. All materials were used with no further treatment. The distilled water used in all measurements was obtained from a Milli-Q Direct 8 Purification System (Merck-Millipore, Molsheim, France).

3.2. Fabrication of Carbon Spheres (CSs)

A quantity of 4.0 g of glucose was dissolved in 50 mL of deionized water and then added to a 100 mL autoclave reactor. The reactor was sealed and heated in a furnace, in which the temperature was gradually increased to 200 °C over 60 min, and then this temperature was held for 10 h prior being allowed to cool to ambient temperature. The carbon spheres were collected by filtration, followed by rinsing several times with deionized water followed by ethanol, before being dried at 80 °C overnight. The CSs were calcined for 5 h at 700 °C with a heating rate of 5°/min in a tube furnace under a nitrogen atmosphere.

3.3. Synthesis of Ni@CS Composite

The microwave irradiation technique was applied to synthesize the composite materials. The CSs (1 g) were first sonicated for 2 h in deionized water (50 mL) until a homogenous dispersion was produced. After that, a certain amount of $Ni(NO_3)_2$ $6H_2O$ was added, followed by 2 h of continuous sonication. While sonicating this suspension, a 1 wt% solution of polyvinyl alcohol (PVA, Mw = 10,000, 80%) as a capping agent was also introduced. The solution was placed in a microwave oven after the addition of 100 μL of hydrazine hydrate. The microwave oven was then run at the highest output in 60-second cycles, for a total reaction time of 240 s (on for 30 s, off and stirring for 30 s). Finally, the Ni@CS catalyst was separated, followed by washing with deionized water and drying at 110 °C for about 10 h. Different Ni loadings were synthesized and assigned as X% CSs, where X (5 and 10%) denotes the Ni percent ratio on the CSs.

3.4. Characterization

X-ray diffraction (XRD) was performed at 40 kV and 40 mA with Cu-K radiation on a Maxima–X (D/Max2500VB2+/Pc, Shimadzu Company, Kyoto 604-8511, Japan) diffractometer. A Shimadzu IR Tracer-100 was used to capture FT-IR spectra in the 400–4000 cm^{-1} region (Shimadzu, 1 Nishinokyo Kuwabara-cho, Nakagyo-ku, Kyoto 604-8511, Japan). On a K-ALPHA (Thermo Fisher Scientific GmbH, Dreieich, Germany) with monochromatic X-ray Al K-alpha radiation -10 to 1350 eV, spot size 400 micro at a pressure of 10^{-9} mbar with full-spectrum pass energy 200 eV and a narrow spectrum 50 eV, X-ray photoelectron spectroscopy (XPS) experiments were performed. A NOVA 4200e (Quantachrome Instruments, Quantachrome GmbH & Co. KG, Boynton Beach, USA) was used to obtain the N_2 isotherms and surface properties at 77 K. TGA profiles (25–600 °C, 10 °C min^{-1}, air

atmosphere) were performed using a Shimadzu TGA-51. Field emission scanning electron microscopy was used to analyze the catalyst morphologies (FESEM, Thermo Scientific Quattro ESEM, Thermo Fisher, Waltham, MA, USA). A JEOL 2100 electron microscope operating at 200 kV was used to obtain high-resolution transmission electron microscopy (HRTEM) images. The nickel content was determined using an iCE3300 AAS atomic absorption spectrophotometer (Thermo Fisher).

3.5. Epoxidation Performance

Typically, a Pyrex tube (20 mL) was supplied with the catalyst composite (50 mg) and alkene (2 mL), H_2O_2 (30%, 2 mL), and $NaHCO_3$ (2 mmol, 0.17 g). The reaction blend was heated to 353 K while being stirred. To attain the highest conversion and selectivity, the temperature, pH, solvent kind (acetonitrile or ethanol), and catalyst dose were adjusted. To confirm the accuracy of the data, each of the catalytic experiments was performed in triplicate, and the averages of the findings were reported. A gas-chromatographic investigation, using an Agilent 6890-N fitted with a capillary column (HP-5 and phenylmethyl siloxane) with a FID detector, was performed throughout the planned period of each experiment. The various by-products were detected using an Agilent GC-MS. The following equations were used to compute conversion and selectivity:

$$\text{Conversion} \% = \frac{\text{Converted Alkene (mole)}}{\text{Alkene (mole)}} 100 \tag{1}$$

$$\text{Selectivity} \% = \frac{\text{Epoxide (mole)}}{\text{Converted alkene (mole)}} 100 \tag{2}$$

4. Conclusions

In conclusion, the Ni@CSs composite successfully catalyzed the epoxidation process of different olefins utilizing H_2O_2-$NaHCO_3$ in an aqueous medium, thus eliminating the need for precious metals, such as Pd. The catalytic investigation displayed that Ni@CSs containing nickel NPs with an average particle size of 26 nm are significantly active for an epoxidation reaction. Furthermore, in an aqueous medium, Ni@CSs were stable and could be recycled for five runs without a noticeable loss in activity.

Data Availability Statement: The data that support the findings of this study are available within the article.

Conflicts of Interest: The author declares no conflict of interest.

References

1. Madubuonu, N.; Aisida, S.O.; Ali, A.; Ahmad, I.; Zhao, T.-K.; Botha, S.; Maaza, M.; Ezema, F.I. Biosynthesis of iron oxide nanoparticles via a composite of Psidium guavaja-Moringa oleifera and their antibacterial and photocatalytic study. *J. Photochem. Photobiol. B Biol.* **2019**, *199*, 111601. [CrossRef] [PubMed]
2. Aisida, S.O.; Akpa, P.A.; Ahmad, I.; Zhao, T.-K.; Maaza, M.; Ezema, F.I. Bio-inspired encapsulation and functionalization of iron oxide nanoparticles for biomedical applications. *Eur. Polym. J.* **2020**, *122*, 109371. [CrossRef]
3. Javed, R.; Zia, M.; Naz, S.; Aisida, S.O.; Ain, N.U.; Ao, Q. Role of capping agents in the application of nanoparticles in biomedicine and environmental remediation: Recent trends and future prospects. *J. Nanobiotechnol.* **2020**, *18*, 172. [CrossRef] [PubMed]
4. Berseth, P.A.; Harter, A.G.; Zidan, R.; Blomqvist, A.; Araújo, C.M.; Scheicher, R.H.; Ahuja, R.; Jena, P. Carbon Nanomaterials as Catalysts for Hydrogen Uptake and Release in $NaAlH_4$. *Nano Lett.* **2009**, *9*, 1501–1505. [CrossRef] [PubMed]
5. Baharudin, L.; Yip, A.; Golovko, V.; Watson, M.J. Potential of metal monoliths with grown carbon nanomaterials as catalyst support in intensified steam reformer: A perspective. *Rev. Chem. Eng.* **2018**, *36*, 459–491. [CrossRef]
6. Testa, C.; Zammataro, A.; Pappalardo, A.; Sfrazzetto, G.T. Catalysis with carbon nanoparticles. *RSC Adv.* **2019**, *9*, 27659–27664. [CrossRef]
7. González-González, R.B.; Rodríguez-Hernández, J.A.; Araújo, R.G.; Sharma, P.; Parra-Saldívar, R.; Ramirez-Mendoza, R.A.; Bilal, M.; Iqbal, H.M. Prospecting carbon-based nanomaterials for the treatment and degradation of endocrine-disrupting pollutants. *Chemosphere* **2022**, *297*, 134172. [CrossRef]

8. Xia, D.; Yu, H.; Li, H.; Huang, P.; Li, Q.; Wang, Y. Carbon-based and carbon-supported nanomaterials for the catalytic conversion of biomass: A review. *Environ. Chem. Lett.* **2022**, *20*, 1719–1744. [CrossRef]

9. Chattopadhyay, J.; Pathak, T.S.; Pak, D. Heteroatom-Doped Metal-Free Carbon Nanomaterials as Potential Electrocatalysts. *Molecules* **2022**, *27*, 670. [CrossRef]

10. Behera, P.; Subudhi, S.; Tripathy, S.P.; Parida, K. MOF derived nano-materials: A recent progress in strategic fabrication, characterization and mechanistic insight towards divergent photocatalytic applications. *Co-ord. Chem. Rev.* **2022**, *456*, 214392. [CrossRef]

11. Pasinszki, T.; Krebsz, M.; Lajgut, G.G.; Kocsis, T.; Kótai, L.; Kauthale, S.; Tekale, S.; Pawar, R. Copper nanoparticles grafted on carbon microspheres as novel heterogeneous catalysts and their application for the reduction of nitrophenol and one-pot multicomponent synthesis of hexahydroquinolines. *New J. Chem.* **2018**, *42*, 1092–1098. [CrossRef]

12. Masteri-Farahani, M.; Modarres, M. Clicked graphene oxide as new support for the immobilization of peroxophosphotungstate: Efficient catalysts for the epoxidation of olefins. *Colloids Surf. A Physicochem. Eng. Asp.* **2017**, *529*, 886–892. [CrossRef]

13. Masteri-Farahani, M.; Mirshekar, S. Covalent functionalization of graphene oxide with molybdenum-carboxylate complexes: New reusable catalysts for the epoxidation of olefins. *Colloids Surf. A Physicochem. Eng. Asp.* **2018**, *538*, 387–392. [CrossRef]

14. Weerakkody, C.; Biswas, S.; Song, W.; He, J.; Wasalathanthri, N.; Dissanayake, S.; Kriz, D.A.; Dutta, B.; Suib, S.L. Controllable synthesis of mesoporous cobalt oxide for peroxide free catalytic epoxidation of alkenes under aerobic conditions. *Appl. Catal. B Environ.* **2018**, *221*, 681–690. [CrossRef]

15. Wang, X.; Wu, G.; Wang, F.; Wei, W.; Sun, Y. Preparation of immobilized chromium Schiff base complexes and their catalytic performance for cyclohexene epoxidation. *Chin. J. Catal.* **2011**, *32*, 1812–1821. [CrossRef]

16. Nasseri, M.A.; Allahresani, A.; Raissi, H. Mild oxidation of alkenes catalyzed by Fe_3O_4/SiO_2 nanoparticles. *React. Kinet. Mech. Catal.* **2014**, *112*, 397–408. [CrossRef]

17. Ghiami, S.; Nasseri, M.A.; Allahresani, A.; Kazemnejadi, M. $FeNi_3@SiO_2$ nanoparticles: An efficient and selective heterogeneous catalyst for the epoxidation of olefins and the doxidation of sulfides in the presence of meta-chloroperoxybenzoic acid at room temperature. *React. Kinet. Mech. Catal.* **2019**, *126*, 383–398. [CrossRef]

18. Samanta, S.; Laha, S.; Mal, N.; Bhaumik, A. Co(III)-containing mesoporous silica as an efficient catalyst in selective dihydroxylation of cyclohexene. *J. Mol. Catal. A Chem.* **2004**, *222*, 235–241. [CrossRef]

19. Samanta, S.; Mal, N.; Bhaumik, A. Mesoporous Cr-MCM-41: An efficient catalyst for selective oxidation of cycloalkanes. *J. Mol. Catal. A Chem.* **2005**, *236*, 7–11. [CrossRef]

20. Held, A.; Kowalska-Kuś, J.; Nowińska, K.; Góra-Marek, K. MCF material as an attractive support for vanadium oxide applied as a catalyst for propene epoxidation with N_2O. *Catal. Lett.* **2018**, *148*, 2058–2068. [CrossRef]

21. De Vos, D.E.; de Wildeman, S.; Sels, B.F.; Grobet, P.J.; Jacobs, P.A. Selective Alkene Oxidation with H_2O_2 and a Heterogenized Mn Catalyst: Epoxidation and a New Entry to Vicinal cis-Diols. *Angew. Chem. Int. Ed.* **1999**, *38*, 980–983. [CrossRef]

22. Hosoya, N.; Hatayama, A.; Irie, R.; Sasaki, H.; Katsuki, T. Rational design of Mn-Salen epoxidation catalysts: Preliminary results. *Tetrahedron* **1994**, *50*, 4311–4322. [CrossRef]

23. Mohamed, S.K.; Abuelhamd, M.; Allam, N.K.; Shahat, A.; Ramadan, M.; Hassan, H.M. Eco-friendly facile synthesis of glucose–derived microporous carbon spheres electrodes with enhanced performance for water capacitive deionization. *Desalination* **2020**, *477*, 114278. [CrossRef]

24. Graf, D.; Molitor, F.; Ensslin, K.; Stampfer, C.; Jungen, A.; Hierold, C.; Wirtz, L. Spatially Resolved Raman Spectroscopy of Single- and Few-Layer Graphene. *Nano Lett.* **2007**, *7*, 238–242. [CrossRef] [PubMed]

25. Zhou, G.; Wang, D.-W.; Yin, L.-C.; Li, N.; Li, F.; Cheng, H.-M. Oxygen Bridges between NiO Nanosheets and Graphene for Improvement of Lithium Storage. *ACS Nano* **2012**, *6*, 3214–3223. [CrossRef]

26. Peng, C.; Lu, X.-H.; Ma, X.-T.; Shen, Y.; Wei, C.-C.; He, J.; Zhou, D.; Xia, Q.-H. Highly efficient epoxidation of cyclohexene with aqueous H2O2 over powdered anion-resin supported solid catalysts. *J. Mol. Catal. A Chem.* **2016**, *423*, 393–399. [CrossRef]

27. Zhan, W.; Guo, Y.; Wang, Y.; Liu, X.; Guo, Y.; Wang, Y.; Zhang, Z.; Lu, G. Synthesis of lanthanum-doped MCM-48 molecular sieves and its catalytic performance for the oxidation of styrene. *J. Phys. Chem. B* **2007**, *111*, 12103–12110. [CrossRef]

28. Pescarmona, P.P.; Jacobs, P.A. A high-throughput experimentation study of the epoxidation of alkenes with transition-metal-free heterogeneous catalysts. *Catal. Today* **2008**, *137*, 52–60. [CrossRef]

29. Valand, J.; Parekh, H.; Friedrich, H.B. Mixed Cu–Ni–Co nano-metal oxides: A new class of catalysts for styrene oxidation. *Catal. Comm.* **2013**, *40*, 149–153. [CrossRef]

30. Sinclair, P.E.; Catlow, C.R.A. Quantum Chemical Study of the Mechanism of Partial Oxidation Reactivity in Titanosilicate Catalysts: Active Site Formation, Oxygen Transfer, and Catalyst Deactivation. *J. Phys. Chem. B* **1999**, *103*, 1084–1095. [CrossRef]

31. Hassan, H.; Betiha, M.A.; El-Sharkawy, E.; Elshaarawy, R.F.; El-Assy, N.; Essawy, A.A.; Tolba, A.; Rabie, A.M. Highly selective epoxidation of olefins using vanadium (IV) schiff base- amine-tagged graphene oxide composite. *Colloids Surfaces A Physicochem. Eng. Asp.* **2020**, *591*, 124520. [CrossRef]

32. Moghe, K.; Sutar, A.K.; Kang, I.K.; Gupta, K.C. Poly(vinylbenzyl chloride-*co*-divinyl benzene) polyHIPE monolith-supported *o*-hydroxynaphthaldehyde propylenediamine Schiff base ligand complex of copper(ii) ions as a catalyst for the epoxidation of cyclohexene. *RSC Adv.* **2019**, *9*, 30823–30834. [CrossRef] [PubMed]

33. Sreethawong, T.; Yamada, Y.; Kobayashi, T.; Yoshikawa, S. Catalysis of nanocrystalline mesoporous TiO_2 on cyclohexene epoxidation with H_2O_2: Effects of mesoporosity and metal oxide additives. *J. Mol. Catal. A Chem.* **2005**, *241*, 23–32. [CrossRef]

34. Jhung, S.H.; Lee, J.-H.; Cheetham, A.K.; Férey, G.; Chang, J.-S. A shape-selective catalyst for epoxidation of cyclic olefins: The nanoporous nickel phosphate VSB-5. *J. Catal.* **2006**, *239*, 97–104. [CrossRef]

35. Ebadi, A.; Mozaffari, M.; Shojaei, S. Aerobic oxidation of cyclohexene catalyzed by NiO/MCM-41 nanocomposites in the gas phase. *J. Chem. Sci.* **2014**, *126*, 989–996. [CrossRef]

36. Hassan, H.M.; Saad, E.M.; Soltan, M.S.; Betiha, M.A.; Butler, I.S.; Mostafa, S.I. A palladium(II) 4-hydroxysalicylidene Schiff-base complex anchored on functionalized MCM-41: An efficient heterogeneous catalyst for the epoxidation of olefins. *Appl. Catal. A Gen.* **2014**, *488*, 148–159. [CrossRef]